

## An *in situ* study using anomalous wide angle X-ray scattering and X-ray absorption spectroscopy of the binary metal oxide catalytic system $\text{SnO}_2\text{-ZnAl}_2\text{O}_4$ supported on alumina

R. Revel, D. Bazin, B. Bouchet-Fabre, A. Seigneurin<sup>1</sup> and Y. Kihn<sup>2</sup>

LURE, Université Paris XI, bâtiment 209D, 91405 Orsay, France

<sup>1</sup> Rhodia, Centre de Recherches d'Aubervilliers, 52 rue de la Haie Coq, 93308 Aubervilliers cedex, France

<sup>2</sup> CEMES-CNRS, BP. 4347, 31055 Toulouse cedex 04, France

**Abstract :** A fine structural description of the local order around zinc and tin atoms of a binary metal oxide catalyst, namely  $\text{SnO}_2\text{-ZnAl}_2\text{O}_4/\text{Al}_2\text{O}_3$  which can be used as a  $\text{DeNO}_x$  catalyst, is achieved through XAS (X-ray absorption Spectroscopy) and AWAXS (Anomalous wide angle X-ray scattering). The analysis of the data was supported by *ab initio* calculations based on the multiple scattering processes for the XAS spectroscopy and *ab initio* calculations based on the Debye equation in the case of anomalous scattering. We found that the tetrahedral sites occupied by the zinc atoms are not completely filled and that part of the zinc atoms are engaged in a  $\text{SnO}_2$  like structure. Also, it seems that most of the tin atoms are engaged in tin dioxide clusters. For the set of *in situ* XAS experiments done at the K Zn edge and K Sn edge, no significant modification of the interatomic distances around each of the two metals versus the reactive gases are measured. Taking into account the previous results obtained on the monoxide metal supported catalyst  $\text{ZnAl}_2\text{O}_4/\text{Al}_2\text{O}_3$ , we can assume thus that only a dramatic lack of occupancy on the metal site favours an incursion of light atoms in the network. This structural property can explain in return the expansion of the crystallographic cell as well as a significant increased of the Debye-Waller factor associated to zinc-zinc pairs.

**Résumé :** Une description détaillée de l'ordre local autour du zinc et de l'étain est effectuée sur un catalyseur  $\text{SnO}_2\text{-ZnAl}_2\text{O}_4/\text{Al}_2\text{O}_3$  par deux techniques spécifiques au rayonnement synchrotron, la spectroscopie d'absorption X et la diffraction anormale. Une attention particulière est portée sur l'analyse des données. En ce qui concerne la spectroscopie d'absorption X, celle-ci s'effectue par le biais de logiciels prenant en compte les processus de diffusion multiple du photoélectron. La simulation numérique des différentielles obtenues par soustraction des diagrammes de diffraction s'effectue à partir de l'équation de Debye en tenant compte des fluctuations du facteur de diffusion atomique en fonction de l'énergie du photon incident. Le jeu de résultats ainsi recueilli permet une mesure précise de l'état électronique du zinc, du taux d'occupation des sites tétraédriques ainsi que de la taille du cristallite de l'oxyde étudié. Se basant sur des résultats précédents inhérents au monométallique  $\text{ZnAl}_2\text{O}_4/\text{Al}_2\text{O}_3$ , nous discutons l'importance du caractère lacunaire en zinc du catalyseur et la relation existant entre cette spécificité et la modification des paramètres structuraux enregistrés à haute température.

## 1. INTRODUCTION

In order to control the emissions of nitrogen oxides in the flue gases from cars [1,2] as well as from power plants and stationary sources, different families of materials have been developed [3,4]. More precisely, several works deal with the catalytic behaviour of spinel materials [see for example ref. 5] but only a few ones try to link their specific catalytic properties to structural characteristics. In a previous work [6], a Xas (X-ray absorption spectroscopy) [7,8] - Amax (Anomalous wide angle X-ray scattering) [9,10] combined approach [11,12,13] was used for the supported system  $\text{ZnAl}_2\text{O}_4/\text{Al}_2\text{O}_3$ .

The use of this experimental approach [14,15] knows now a tremendous expansion with the development of experimental set-ups completely dedicated to study such low-ordered materials and equipped with special reaction cells in order to mimic different chemical reactions [16,17]. The different publications in the field of heterogeneous catalysis [18,19] for example demonstrate clearly that these *in situ* studies are mostly important as they provide essential information on the real catalyst and temperature as well as the nature of the reactive gas are there parameters to take into account [20, 21].

For the supported system  $\text{ZnAl}_2\text{O}_4/\text{Al}_2\text{O}_3$ , this family of compounds has been the subject of several studies since it has been used for adsorption and conversion of methanol [22,23]. In our case [6], among the different key results, we have found a significant lack of occupancy on the tetrahedral zinc site. This structural characteristic seems to favour an incursion of light atoms in the zinc network which can explain in return the expansion of the crystallographic cell associated to zinc atoms as well as the significant increase of the Debye-Waller factor associated to zinc-zinc pairs.

Here, through a study of a binary metal oxide supported system  $\text{SnO}_2\text{-ZnAl}_2\text{O}_4/\text{Al}_2\text{O}_3$ , we want to evaluate the influence of the second oxide metal namely  $\text{SnO}_2$  on the spinel like environment of zinc. More precisely, we would like to determine if the expansion of the interatomic distance Zn-Zn at 3.50 Å as well as the dramatic increase of the Debye-Waller factor associated to Zn-Zn pairs are still measured at 500°C for this binary metal oxide. In a same way, a similar approach is done for the tin atoms in order to describe the phase in which these atoms are engaged. Following the same procedure used for the  $\text{ZnAl}_2\text{O}_4/\text{Al}_2\text{O}_3$  sample [see for more details reference 6], the supported catalytic system  $\text{SnO}_2\text{-ZnAl}_2\text{O}_4/\gamma\text{-Al}_2\text{O}_3$  which have been selected for this study has been provided by Rhodia.

## 2. EXPERIMENTAL SECTION

### 2.1 X-ray Diffractometer

Classical X-ray powder pattern were recorded at the Centre de Recherches de Rhodia in Aubervilliers by using  $\text{Cu K}\alpha$  radiation ( $\lambda = 1.5418 \text{ \AA}$ ) generated at 40 KeV with a current of 40 mA on a vertical X-ray diffractometer (Philips PW 1800). This apparatus was equipped with automatic variable slits, diffracted beam graphite monochromator, proportional counter, and pulse height analyser. A scan speed of  $0.2^\circ 2\theta/\text{s}$  was used.

Diffraction experiments [9] were also done at LURE (Laboratoire pour 'Utilisation du Rayonnement Synchrotron), the French photon factory in Orsay using the synchrotron radiation from the D.C.I. storage ring running at 1.85 GeV with a current of 300 mA and a time life of 200 hours. The diffraction diagrams were collected on the W 31 wiggler beamline equipped with a Si 111 double crystal monochromator. The energy calibration was made by recording the fluorescence of the sample and compare to Xas measurements done in transmission. To limit the

variation of the absorption coefficient,  $\theta/2\theta$  scanning in the range  $0.5 < q < 8.5 \text{ \AA}^{-1}$  was performed at 9200.eV and 9661. eV and thus below the zinc K edge .

The incident beam was limited by an entrance slit of 2 mm \* 4 mm and monitored by an ionisation detector. The scattered beam was collected by a 12 pixels solid state detector which allows to register simultaneously 12 spectra at each angular scan. This experimental improvement compared to the classic NaI scintillation detector yield, in about 8 hours of measurements differential intensities with a low noise level of a few per cent even for a low concentrated atomic species material [24].

## 2.2 Electron Microscopy

The electron microscope used was a JEOL 100 system with a Kevex energy dispersive X-ray spectrometer for the AEM analysis. The samples for electron microscopy were made using a microtomy device. The microscope was operating at different direct magnification.

## 2.3 Xas Spectrometer

The Xas spectra were performed at LURE on the Exafs IV beam line positioned after a bending magnet [25]. The X-rays were monochromatized by two silicium (311) single crystals for the zinc K edge and by two germanium (400) for the tin K edge. This monochromator, operating with 1 mm vertical slits, has an energy resolution at 10KeV of 2.3eV and at 30KeV of more than 10. eV. The incident  $I_0$  and transmitted  $I_1$  intensities were recorded by use of two ionisation chambers filled with argon (for the zinc K edge) or krypton (for the tin K edge). Calibration of the different experiments were made with a reference zinc metal foil (9659.eV) or a reference tin metal foil (29200.eV) using the reference X-ray spectra of different metal foils.

The catalysts were in powder form screened to 100-200  $\mu\text{m}$  and the Xas spectra were recorded by placing appropriate quantity of the sample in thin carbon frame. Details on the different apparatus used in this study can be found in reference 26. The absorber thickness of the different samples was chosen such that  $\mu x = 1$  ( $\mu$  is the linear absorption coefficient,  $x$  is the thickness) for the zinc K edge and such that  $\mu x = 0.6$  for the tin K edge. Finally, particular attention was taken in order to make the samples of homogeneous thickness.

The Exafs oscillations were extracted according to a classical procedure. Background subtraction, normalisation by the jump height at the K edge of the raw data, Fourier Transform (F.T.) uncorrected from phase shift were performed using the program written by A. Michalowicz [27]. Numerical refinements have been done using a simplex code [27] or using FeFF fit [28]. The shell occupation number and disorder parameters are highly correlated typically prevented the coordination number from being determined to a precision better than  $\pm 1$ . The error in bond length is estimated to be of the order of  $\pm 0.03 \text{ \AA}$  for the nearest neighbour shell. For all simulations, the edge shift  $\Delta E$  was maintained at a value less than 4 eV [29]. During the chemical treatment, the catalyst is treated under a flow of 330vpmNO/330vpmC<sub>3</sub>H<sub>6</sub>/370vpmCO/11%O<sub>2</sub>/11%CO<sub>2</sub>/balance N<sub>2</sub> for a VVH of 10 000 h<sup>-1</sup> for the experiments done at the zinc K edge and 2 000 h<sup>-1</sup> for the experiments done at the tin K edge. Control of the flow is done by measuring the pressure and the massflow after the sample. The temperature of the sample was then increased up to 500°C and the Xas spectra were recorded *in situ* at different temperatures (30°C, 300°C, 400°C, 500°C, 30°C) at the Zn K edge and at the Sn K edge. A similar experiment has been done without the reactive gases mixture in order to distinguish between the effect of the two parameters (gases and temperature). On line data analysis up to the

Fourier transform was used in order to check that the chemical reaction was proceeding. It shows that under our experimental conditions, 2 hours was sufficient to complete the reactions.

### 3. THEORETICAL BACKGROUND

#### 3.1 Theory of Anomalous Wide Angle X-ray Scattering

The ordinary X-ray scattering methods are not atom selective, so that the scattering effects from the oxide particles and the support superpose. They can be separated reliably only if the diffraction peaks associated with the catalyst particle are sufficient sharp and the scattering from the support sufficiently featureless. This limitation can be avoided easily by using the anomalous scattering technique for which we recall now some basic aspects [30,31,32]. Assuming a random (powder) arrangement of the structure with respect to the incoming X-ray beam, for a multiatom system, the intensity of coherently scattered X-rays is given by

$$I(q) = \sum_i \sum_j f_i(q) f_j(q) \sin(qR_{ij})/qR_{ij} \quad \text{with } f(q) = f_0(q) + f'(E) + if''(E) \quad (1)$$

In this equation,  $I(q)$  is the angle dependent intensity from coherent scattering, the sums over  $i$  and  $j$  are over all the atoms,  $R_{ij}$  being the distance between the atom  $i$  and  $j$  and  $f_i$  and  $f_j$  being the angle dependent atomic scattering factors. Thus, for a structure in which all of the atomic positions have been specified, the diffraction intensity can be directly calculated using the Debye equation [11].

Anomalous scattering methods use the variation of the atomic scattering power as a function of photon energy near inner shell absorption edges. For the classical part,  $f_0(q)$ , we use the Cromer and Mann parameters [33]. Moreover, special attention is paid for the determination of the dispersive factor  $f'$  [34] which was carried out using also the photoelectronic cross section  $\mu$  and the optical theorem and the evaluation of  $f''$  which was made using the Kramers-Kronig relationship (see for details ref. 35 and 36). Finally, for the analysis part, we will proceed to a precise comparison between the experimental signals and numerical simulations [11,37,38].

#### 3.2 Theory of the X-ray absorption spectroscopy

The different aspects of the analysis procedure of experimental Exafs data have been already discussed in details [39] and particularly the necessity to take into account multiple scattering processes [40, 41]. In these conditions, the Exafs spectrum is written as a sum of different multiple scattering contributions and each such contribution can be written in the form

$$\chi_n(k) = \chi_0^n(k) \exp(-L_n/\lambda_n - 2k^2\sigma^2) \quad \text{and} \quad \chi_0^n(k) = F_n(k) \sin(kL_n + \theta_n(k)) \quad (2)$$

here  $n$  represents different single or multiple scattering paths and  $L_n$  is the total path length.  $F_n(k)$  and  $\theta_n(k)$  are the amplitude and phase which depend on  $k$ , on the scattering path involved and on the atomic potential parameter.

Above the first shell, multiple scattering contributions cannot be systematically neglected and may in certain cases even be dominant. More precisely, multiple scattering contributions cannot be neglected in the case of the reference compound  $ZnAl_2O_4$  [6].

#### 4. REFERENCE COMPOUNDS

Results regarding the reference compound  $ZnAl_2O_4$  have been already presented [6,42]. We just recall that in this phase the zinc atoms occupy a tetrahedral site and are thus surrounded by 4 oxygen atoms situated at 1.95 Å. The second coordination sphere is made of aluminium atoms ( $N=12$  at  $R=3.35$  Å), oxygen atoms ( $N=12$  at  $R=3.39$  Å) and zinc atoms ( $N=4$  at  $R=3.50$  Å). For the tin dioxide, figure 1 shows the classical XRD diagram ( $\lambda = 1.5418$  Å) from which the structural parameters have been extracted using a Rietveld method (table I). The different structural results obtained in this study are in line with the previous data given by A. Winchella et al. [43].

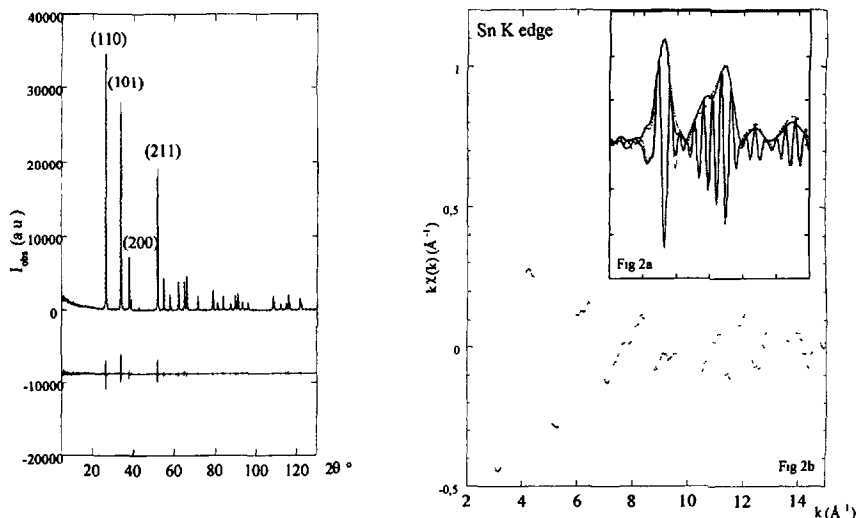


**Figure 1:** Classical diffraction diagram (line) and its Rietveld simulation (dots) for the compound  $SnO_2$ .

Diagramme de diffraction (ligne) et sa simulation Rietveld (pointillé) pour le composé  $SnO_2$

**Figure 2:** Exafs modulations (Fig 2a) and F T. Modulus (Fig 2b) at the K Sn edge of the compound  $SnO_2$ .

Modulations Exafs et transformée de Fourier obtenue au seuil K de l'étain pour le composé  $SnO_2$ .

**Table I:** Structural parameters obtained for the reference compound  $SnO_2$  through a numerical simulation of the experimental diagram using a Rietveld method.

Paramètres structuraux obtenus pour le composé  $SnO_2$  à partir de la simulation Rietveld du diagramme de diffraction.

$\lambda$ (Å)	1.5418 Å	
step ( $^{\circ}2\theta$ )	0.05	
angular range ( $^{\circ}2\theta$ )	7-130	
Number of diffraction peaks	47	
Rp	9.61	
Rwp	9.83	
$\chi^2$	3.5	
RB	4.76	
RF	4.38	
$\lambda$ (Å)	1.54766	
$f'(e)$	-2.72	
$f''(e)$	0.53	
cell parameters (Å)	a = 4.73720(6) b = 4.73720(6) c = 3.18624(5)	
Atoms	x, y, z	$B_{iso}$ (Å)
Sn	0., 0., 0.	0.59(2)
O	0.3034(7) 0.3034(7) 0.0	0.7(1)

Figure 2a shows the Exafs modulations after the K edge tin (29200 .eV) of the tin dioxide reference compound as a function of energy after removing the background. F.T. modules of the experimental data compare to the numerical simulation (gathered in table II) have been plotted also on figure 2b in order to show the high quality of the numerical simulation.

**Table II :** Structural parameters which were used in the fitting procedure of the Exafs modulations associated to the reference compound spinelle SnO<sub>2</sub>.

Paramètres structuraux obtenus par simulation numérique des modulations Exafs du spectre d'absorption X collectés au Seuil K de l'étain pour le composé SnO<sub>2</sub>.

Number	Bond	Distance (Å)
2	Sn-O	2.0326
4	Sn-O	2.0671
2	Sn-Sn	3.1862
4	Sn-O	3.5993
8	Sn-Sn	3.7093
4	Sn-O	3.7794
8	Sn-O	4.2297
2	Sn-O	4.6668
4	Sn-Sn	4.7372
8	Sn-O	4.8070
4	Sn-O	4.9575
4	Sn-O	5.6131

## 5. EX SITU RESULTS

We first discuss the results observed on the air exposed sample, the SnO<sub>2</sub>-ZnAl<sub>2</sub>O<sub>4</sub>/Al<sub>2</sub>O<sub>3</sub> catalyst, which readily reveal some unusual structural characteristics.

### 5.1 Electron Microscopy

A direct examination of the catalyst with the conventional transmission electron microscope gives evidence of different phases. On a transition alumina which seems to be of  $\gamma$  type, a non homogenous distribution of the zinc atoms is measured. Moreover, grapes of dioxide tin clusters are detected for which the diameter is around 6 nm. These classical observations have been completed by fluorescence measurements which seems to show that tin atoms and zinc atoms are completely demixed as far as fluorescence photons can be detected.

### 5.2 X-ray diffraction

Figure 3 shows the total normalised diffraction pattern obtained at one wavelength ( $\lambda = 1.5418 \text{ \AA}$ ) taken on the classical set up. It is characteristic of a modified alumina with some small features which can be attributed to nanometric size clusters of tin dioxides, namely the diffraction peaks 110, 101 and 211. A simple analysis can be done regarding the diffraction pattern part associated to SnO<sub>2</sub> clusters. The classical Scherrer formula which relates the size of the cluster to the width of the diffraction peak gives a diameter of 2 nm, the measurement being done on the (110) diffraction peak. This rough value is confirmed by numerical simulations of the diffraction diagram using the Debye equation [44] and which show that the presence of a secondary feature cannot be associated to smaller clusters (figure 3). Note that this value of 2 nm is far from the value given by the electronic microscopy equal to 6 nm. At this step of the analysis, this discrepancy can be explained by the existence of a size distribution, the electronic microscopy visualising mostly the bigger particles.

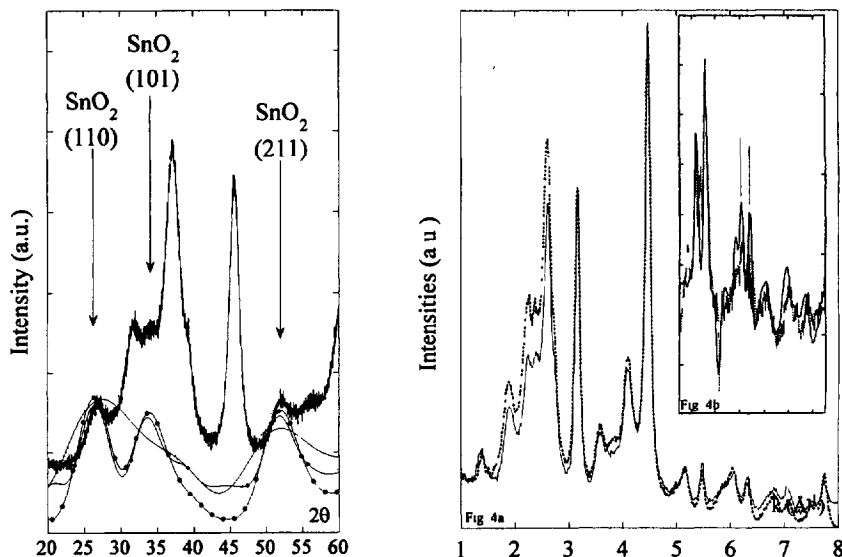


**Figure 3:** Classical XRD diagram of the catalyst  $\text{SnO}_2\text{-ZnAl}_2\text{O}_4/\text{Al}_2\text{O}_3$  compared to ab initio calculations of  $\text{SnO}_2$  cluster having different diameters: 11 Å, line; 15 Å, dots; 20 Å, circles; 26 Å, diamonds

Diagramme de diffraction du catalyseur  $\text{SnO}_2\text{-ZnAl}_2\text{O}_4/\text{Al}_2\text{O}_3$  comparé à différentes simulations correspondant à des agrégats de  $\text{SnO}_2$  de différents diamètres : 11 Å, ligne; 15 Å, points, 20 Å, cercles; 26 Å, diamants.

**Figure 4a:** XRD diagram of the catalyst  $\text{SnO}_2\text{-ZnAl}_2\text{O}_4/\text{Al}_2\text{O}_3$  collected at two energies  $E= 9200. \text{ eV}$  (dots) and  $9661. \text{ eV}$  (line).

Diagramme de diffraction du catalyseur  $\text{SnO}_2\text{-ZnAl}_2\text{O}_4/\text{Al}_2\text{O}_3$  collectés à deux énergies  $E= 9200. \text{ eV}$  (points) and  $9661. \text{ eV}$  (ligne)

**Figure 4b:** Differential intensities of the catalyst (dots) compared to the difference in scattered intensities obtained for the reference compound  $\text{ZnAl}_2\text{O}_4$  (line) for which the major features have been indexed.

Intensité différentielle de l'échantillon  $\text{SnO}_2\text{-ZnAl}_2\text{O}_4/\text{Al}_2\text{O}_3$  (points) comparé à celle du composé de référence  $\text{ZnAl}_2\text{O}_4$  (ligne).

In order to get information relative to the zinc atoms, we have performed two diffraction patterns on a wiggler beam line at two energies just before the Zn K edge for which the energy is at 9664. eV, its electronic state being  $2^+$ . The intensities measured at these two different energies ( $E = 9200. \text{ eV}$  and  $9661. \text{ eV}$ ) are plotted on figure 4a. Figure 4b shows the Das pattern obtained by subtracting the normalised scattered. Due to the low concentration of zinc and also a rather weak change in the scattering factor ( $\Delta f$  is assumed to be equal to approximately), the Das pattern is obviously more noisy. From a rough comparison between the differential associated to the catalyst and the differential obtained for the reference compound  $\text{ZnAl}_2\text{O}_4$ , it is clear that the local order around zinc atom is spinel like.

### 5.3 Xanes and Exafs results

Figure 5a shows the near edge region at the Zn K edge of the catalyst compare to the near edge region associated to the model compounds zinc monoxide and the spinel  $\text{ZnAl}_2\text{O}_4$ . Figure 6a displays the near edge region of the absorption spectrum collected at the Sn K edge for the model compound  $\text{SnO}_2$  and for the catalyst. For these two elements, it is seen that the structure features above the edge between the catalyst and the reference compounds ( $\text{ZnAl}_2\text{O}_4$  and  $\text{SnO}_2$ ) are very similar [45]. Thus, the electronic state of Zn atom is  $2^+$  and the electronic state of Sn atom is  $4^+$ .

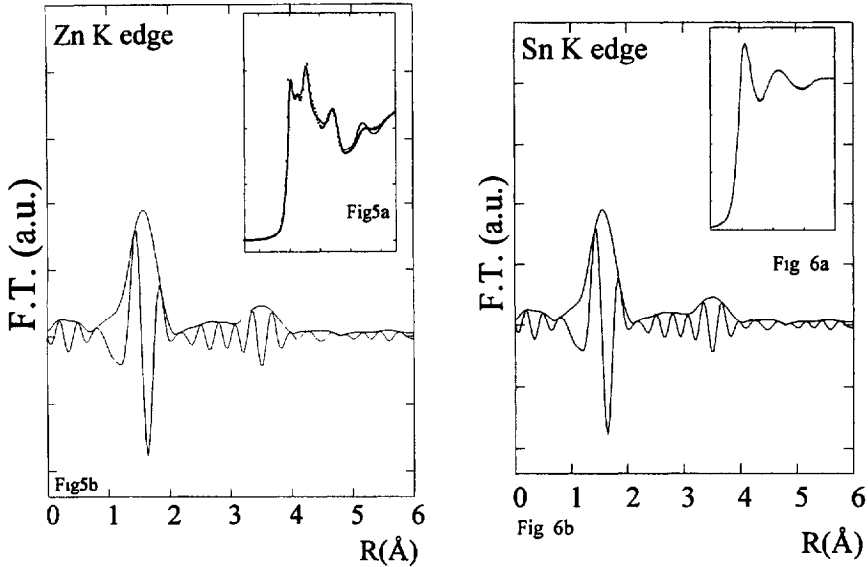


**Figure 5 :** Xanes (Fig5a) and F.T. modules (Fig 5b) at the zinc K edge of the catalyst (square) compare to the near edge region associated to the model compounds ZnO (dashes) and  $ZnAl_2O_4$  (line).

Xanes (Fig 5a) et Modules de transformée de Fourier collectés au seuil K du zinc de l'échantillon (carré) et des composés de référence ZnO (ligne-point) et  $ZnAl_2O_4$  (ligne).

**Figure 6 :** Xanes (6a) and F.T. modules (Fig 6b) at the Sn K edge for the model compound  $SnO_2$  (line) and for the catalyst (dots).

Xanes (Fig 5a) et Modules de transformée de Fourier collectés au seuil K de l'étain de l'échantillon (points) et des composés de référence  $SnO_2$  (ligne)

**Table III :** Structural parameters which were used in the fitting procedure of the Exafs modulations associated to the catalyst  $SnO_2-ZnAl_2O_4/Al_2O_3$  at the Zn K edge for the first set of experiments.

Paramètres structuraux obtenus au seuil K du zinc pour le premier jeu d'expériences effectué sur l'échantillon  $SnO_2-ZnAl_2O_4/Al_2O_3$ .

T(°K)	Zn-O N = 4.		Zn-Al N = 10.9		Zn-O N = 10.3		Zn-Zn N = 2.		Zn-Al-O N = 23.4		Zn-O N = 10.9		Zn-Al-O N = 22.7	
	R(Å)	$\sigma^{2(*)}$	R(Å)	$\sigma^{2(*)}$	R(Å)	$\sigma^{2(*)}$	R(Å)	$\sigma^{2(*)}$	R(Å)	$\sigma^{2(*)}$	R(Å)	$\sigma^{2(*)}$	R(Å)	$\sigma^{2(*)}$
303	1.95	3.5	3.35	6.1	3.39	14.5	3.50	16.1	3.60	2.9	4.27	3.7	4.37	3.7
573	1.96	4.8	3.35	9.4	3.40	18.8	3.50	21.0	3.61	5.3	4.27	5.8	4.38	4.7
673	1.95	5.4	3.35	10.9	3.39	21.8	3.50	27.4	3.61	6.1	4.27	8.0	4.37	5.9
773	1.96	6.3	3.35	12.0	3.39	22.3	3.50	27.7	3.61	7.2	4.27	8.0	4.38	7.0

\* in  $\text{Å}^2 \cdot 10^3$

The F.T. obtained at the Zn K edge for the catalyst at room temperature is presented in figure 5b. The best-fit calculated Exafs parameters characterising the local environment of zinc are summarised in table III. The present Exafs analysis confirm the previous results obtained through the Xanes part. The F.T. associated to the catalyst is very similar to the F.T. of the reference compound spinel  $ZnAl_2O_4$  and is characterised by a first peak at  $1.7\text{Å}$  attributed to Zn-O bonds. The numerical simulation gives for this first shell 4 oxygen atoms at  $1.95\text{Å}$ . The second feature (peak b) of the modulus is assigned to different kind of bonds namely Zn-Al (N = 10.9,

$R = 3.35\text{\AA}$ ), Zn-O ( $N = 10.3$ ,  $R = 3.39\text{\AA}$ ) and Zn-Zn ( $N = 2.$ ,  $R = 3.50\text{\AA}$ ). These two major features are thus a clear fingerprint of a spinel like local order around zinc atoms. The numerical simulations give a more quantitative point of view and clearly, the main result comes from the number of zinc-zinc bonds situated at  $3.50\text{\AA}$  which revealed a weak occupation of tetrahedral site.

**Table IV :** Structural parameters which were used in the fitting procedure of the Exafs modulations associated to the catalyst  $\text{SnO}_2\text{-ZnAl}_2\text{O}_4/\text{Al}_2\text{O}_3$  at the Sn K edge for the first set of experiments.

Paramètres structuraux obtenus au seuil K de l'étain pour le premier jeu d'expériences effectué sur l'échantillon  $\text{SnO}_2\text{-ZnAl}_2\text{O}_4/\text{Al}_2\text{O}_3$ .

T (°C)	$\Delta E$ eV	N Sn-O	R Å	$\sigma^2$ Å <sup>2</sup>	$\Delta E$ eV	N <sub>1</sub> Sn-Sn	R Å	$\sigma^2$ Å <sup>2</sup>	N <sub>2</sub> Sn-Sn	R Å	$\sigma^2$ Å <sup>2</sup>
30	1.6	5.6	2.05	4.4	6.6	1.2	3.19	3.4	4.8	3.72	5.5
300	2.2	6.0	2.04	5.8	4.0	1.2	3.16	4.0	4.8	3.70	9.2
400	2.3	5.9	2.05	6.7	3.9	1.2	3.18	6.2	4.8	3.71	11.4
500	2.5	5.9	2.05	7.1	4.4	1.2	3.16	9.6	4.8	3.71	13.9
30	2.3	5.6	2.05	4.5	2.9	1.2	3.18	3.0	4.8	3.70	6.4

$$\Gamma = 0.46\text{\AA}^{-2}$$

The results obtained at the Sn K edge are shown on figure 6b for the F.T. In the F.T. module, the first peak which is dominant is associated to tin oxygen bonds and for the second peak, the most important contribution comes from tin-tin bonds. From the numerical simulations gathered in table IV, it is clear that most of the tin atoms are engaged in tin dioxide clusters. The size of the cluster as well as its morphology can be determined from the coordination numbers [46,47]. In our case, a similar relationship can be used to determine the size of the cluster from the coordination number associated to Sn-Sn bonds. We have pointed out that this relationship supposes a complete occupation for the different crystallographic site. A value of 1.5 nm is then found in line with previous value given by the diffraction.

## 6. IN SITU EXAFS RESULTS

The Exafs measurements on the catalyst were obtained in conditions close to their industrial conditions, the reactive gas being a synthetic mixture. In order to separate the possible effect of temperature to the influence of the reactive gases, two sets of experiments have been done.

For the first set, temperature of the sample which varies between 30°C and 500°C is the only parameter which has been changed. Figure 7a and 8a show the different F.T. modules collected either at the Zn K edge or at the Sn K edge during the first experiment. At this point of the analysis, we have to underline that after all the different chemical treatments performed on the catalyst, we have noticed that the structural characteristics are the same before and after the experiment. This fact has imposed that the different coordination numbers are the same for all the numerical refinements we have done.

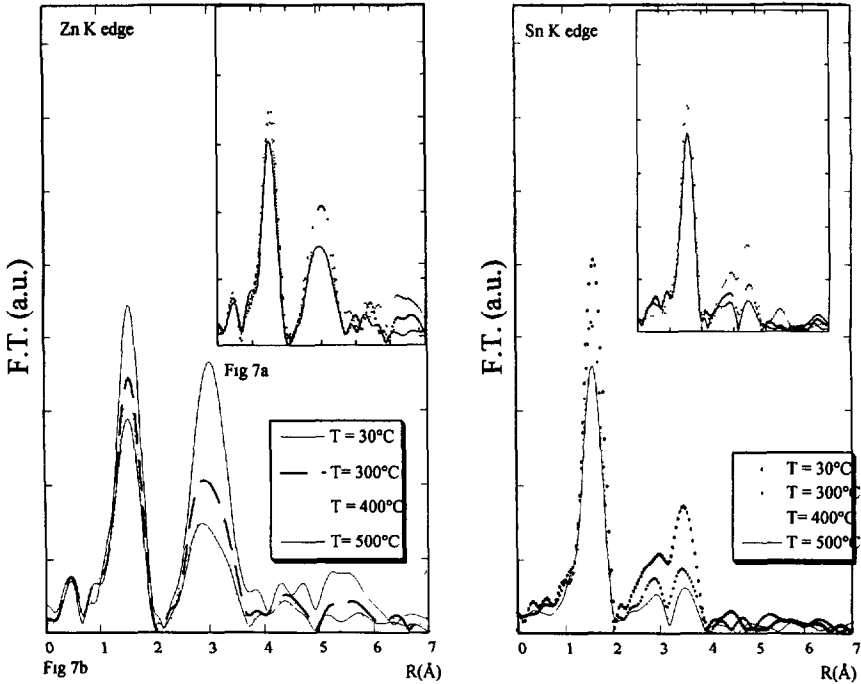


**Figure 7a.** Moduli of the F. T. measured at the K Zn edge and collected at different temperature during the first set of experiments performed on the catalyst (without reactiv gases).

Modules de transformée de Fourier collectés au seuil K du zinc de l'échantillon à différentes températures au cours du premier jeu d'expériences (sans gaz réactifs).

**Figure 7b.** Moduli of the F. T. measured at the K Zn edge and collected at different temperatures during the second set of experiments (with reactiv gases) performed on the catalyst.

Modules de transformée de Fourier collectés au seuil K du zinc de l'échantillon à différentes températures au cours du second jeu d'expériences (avec gaz réactifs).

**Figure 8a.** Moduli of the F. T. measured at the K Sn edge and collected at different temperature during the first set of experiments performed on the catalyst (without reactiv gases)..

Modules de transformée de Fourier collectés au seuil K de l'étain de l'échantillon à différentes températures au cours du premier jeu d'expériences (sans gaz réactifs).

**Figure 8b.** Moduli of the F. T. measured at the K Sn edge and collected at different temperatures during the second set of experiments (with reactiv gases) performed on the catalyst

Modules de transformée de Fourier collectés au seuil K de l'étain de l'échantillon à différentes températures au cours du second jeu d'expériences (avec gaz réactifs).

**Table V :** Structural parameters which were used in the fitting procedure of the Exafs modulations associated to the catalyst  $\text{SnO}_2\text{-ZnAl}_2\text{O}_4/\text{Al}_2\text{O}_3$  at the Zn K edge for the second set of experiments.

Paramètres structuraux obtenus au seuil K du zinc pour le second jeu d'expériences effectué sur l'échantillon  $\text{SnO}_2\text{-ZnAl}_2\text{O}_4/\text{Al}_2\text{O}_3$ .

T(°K)	Zn-O N= 4		Zn-Al N= 10.9		Zn-O N= 10.3		Zn-Zn N= 2		Zn-Al-O N= 23.4		Zn-O N= 10.9		Zn-Al-O N= 22.7	
	R(Å)	$\sigma^{2(*)}$	R(Å)	$\sigma^{2(*)}$	R(Å)	$\sigma^{2(*)}$	R(Å)	$\sigma^{2(*)}$	R(Å)	$\sigma^{2(*)}$	R(Å)	$\sigma^{2(*)}$	R(Å)	$\sigma^{2(*)}$
303	1.95	3.1	3.34	5.8	3.39	13.5	3.49	14.5	3.60	2.4	4.26	3.1	4.37	3.4
573	1.95	5.0	3.35	9.8	3.39	18.5	3.50	20.7	3.61	4.9	4.27	6.0	4.37	4.8
673	1.96	5.5	3.35	11.0	3.39	22.4	3.50	28.7	3.61	7.5	4.27	8.3	4.37	6.1
773	1.96	6.4	3.35	12.2	3.39	23.0	3.50	29.3	3.61	7.1	4.27	8.7	4.37	7.0

\*in  $\text{Å}^2 \cdot 10^3$

As it can be seen, significant modifications are measured associated to the increase of the Debye-Waller factors associated to different kind of bonds. Results obtained after the simulations of the Exafs modulations gathered in table V clearly support this dependence. As we noticed previously, the structural parameters measured at the beginning and at the end of the chemical treatment are the same.

**Table VI :** Structural parameters which were used in the fitting procedure of the Exafs modulations associated to the catalyst  $\text{SnO}_2\text{-ZnAl}_2\text{O}_4/\text{Al}_2\text{O}_3$  at the Sn K edge for the second set of experiments.

Paramètres structuraux obtenus au seuil K de l'étain pour le second jeu d'expériences effectué sur l'échantillon  $\text{SnO}_2\text{-ZnAl}_2\text{O}_4/\text{Al}_2\text{O}_3$ .

T (°C)	$\Delta E$ (eV)	N Sn-O	R (Å)	$\sigma^2$ (Å <sup>2</sup> )	T (°C)	$\Delta E$ (eV)	N <sub>1</sub> Sn-Sn	R (Å)	$\sigma^2$ (Å <sup>2</sup> )	N <sub>2</sub> Sn-Sn	R (Å)	$\sigma^2$ (Å <sup>2</sup> )
30	1.4	5.6	2.05	3.4	30	5.6	1.2	3.19	2.3	4.8	3.71	5.3
300	0.9	5.6	2.05	6.2	300	7.9	1.2	3.19	3.8	4.8	3.70	8.5
400	1.6	5.5	2.05	6.4	400	4.8	1.2	3.18	5.3	4.8	3.70	10.4
500	1.9	5.4	2.05	6.6	500	6.2	1.2	3.17	4.8	4.8	3.70	11.4
30	1.0	5.5	2.05	4.6	30	6.2	1.2	3.18	2.9	4.8	3.71	5.6

$$\Gamma = 0.46 \text{ \AA}^{-2}$$

For the second set of *in situ* experiments, a second experimental parameter is added : the stream of reactive gases passing through the sample. On figure 7b and 8b have been plotted the different F.T. modules collected either at the Zn K edge or at the Sn K edge. One more time, significant changes in the modules are observed. Nevertheless, the effect of the reactive gas seems to be rather small, the different results gathered in table VI obtained for the second experiment being relatively close to the results associated to the first set (table IV). Obviously, the coordination numbers keep their values and the different interatomic distances as well as the Debye-Waller factors are very similar.

## 7. DISCUSSION

From a general point of view, the distribution and the electronic state of cation in a material are among the keys parameters which control the catalytic properties [48,49]. The work done by Ziolkowski et al. [50, 51] on Zn-Mn-Al-O containing spinels illustrates this relationship. More precisely, octahedrally sited  $\text{Mn}^{3+}$  ions are suspected to be active sites for the reduction of nitrobenzene. The X-ray absorption spectroscopy is often used now as a chemical tool to obtain this kind of information. Here, the measurement of the Xanes region shows that the electronic state of Zn atom is  $2^+$ , the electronic state of tin atom being  $4^+$ . Also, a fine analysis of the Exafs modulations give the short range ordering around these two elements, the local order around zinc atoms is identified having a spinel like structure, most of the tin atoms being engaged in tin oxide clusters.

At the opposite of the work done by Otero Arean et al. [52] on spinel type  $\text{ZnAl}_2\text{O}_4$ ,  $\gamma\text{-Al}_2\text{O}_3$  and  $\text{Al}_2\text{O}_3\text{-ZnAl}_2\text{O}_4$  solid solutions, the classical Rietveld method cannot be used in order to extract the lattice parameter. This is due to the fact that the only diffraction peak which can be associated to the  $\text{ZnAl}_2\text{O}_4$  spinel, the (4,2,2) feature is very large and has a very weak intensity. That's why anomalous diffraction technique has been used. Different simulations based on the size of the cluster or the occupation of the different crystallographic site have been done to mimic the differential intensity and they clearly show that the observed diffraction patterns cannot be

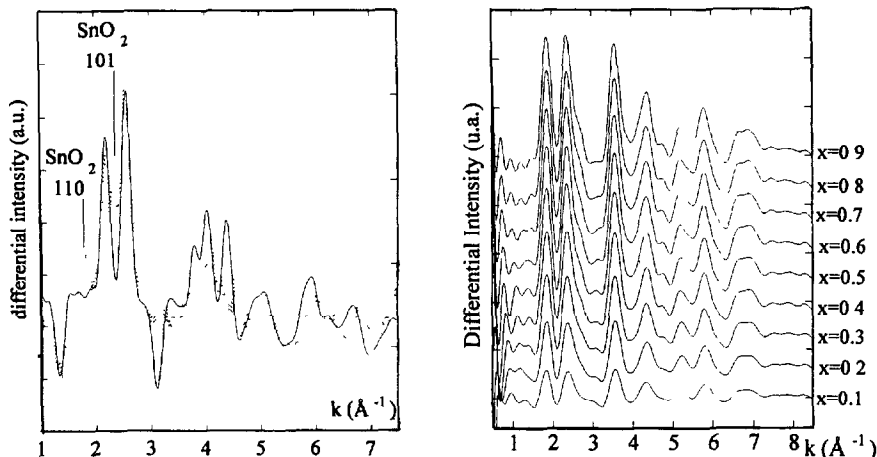


**Figure 9.** Differential intensity measured for the catalyst (dots) compare to a differential associated to a ZnAlO cluster (line) :  $Zn_8Al_{30}O_{53}$

Intensité différentielle mesurée pour le catalyseur (pointillé) comparé à une simulation numérique relative à un agrégat  $Zn_8Al_{30}O_{53}$  (ligne).

**Figure 10.** Differential intensities related to  $Zn_xSn_{1-x}O_{2-x}$  for a cluster of 26 Å diameter.

jeu d'intensités différentielles calculée pour des agrégats  $Zn_xSn_{1-x}O_{2-x}$  diamètre de 26 Å.

simulated assuming only ZnAlO clusters. As reported on figure 9, the best simulation which can be done is associated to a  $ZnAl_2O_4$  cluster containing a very low number of atoms :  $Zn_8Al_{30}O_{53}$ .

In order to simulate the other diffraction features assigned to  $SnO_2$  clusters namely the diffraction features 110, 101 and 211, differential intensities related to  $Zn_xSn_{1-x}O_{2-x}$  for a cluster of 26 Å diameter, with  $0.1 < x < 0.9$ . These differential intensities have been plotted on figure 10. Clearly, the previous features 110, 101 and 211 are now taking into account. This simple analysis shows in fact that part of the zinc atoms are engaged in a  $SnO_2$  like structure and clearly also points out the advantages of the diffraction techniques versus the X-ray absorption spectroscopy for a multiphase sample.

Thus, zinc atoms are part of two structures a spinel like ( $ZnAl_2O_4$ ) one and a cassiterite like ( $SnO_2$ ). Because X-ray absorption spectroscopy made an average between these two structures, it is simply not possible to give evidence of the second one. This study shows thus that a Xas-Awaxs combined approach constitute a major improvement in the determination of the structural characteristics in term of phase analysis at a nanometer scale.

Regarding now the two set of *in situ* experiments (with and without gases), even if the tetrahedral site occupied by the zinc atoms are not completely filled, no significant modification of the interatomic distances as well as the Debye-Waller factor associated to zinc-zinc pairs are measured. The different interatomic distances measured by Exafs associated to zinc - oxygen, zinc-aluminium or zinc - zinc bonds keep their initial values. Also, for tin atoms, the two set experiments have shown that the local order around this metal is unchanged whatever the experimental conditions (with or without gases). Taking into account the results obtained on the monometallic supported catalyst  $ZnAl_2O_4/Al_2O_3$ , we can assume thus that only a dramatic lack of occupancy on the metal site favour an incursion of light atoms in the network which can explain the expansion of the crystallographic cell as well as a significant increased of the Debye-Waller factor associated to zinc-zinc pairs.

## 8. CONCLUSION

We have seen that, a combined Xas-Awaxs approach compare to a more classical one, gives a more detailed description of the dioxide clusters supported on alumina namely the supported system  $SnO_2-ZnAl_2O_4/Al_2O_3$ .

For the tin atoms, the results given by the line broadening analysis for the determination of the averaged  $\text{SnO}_2$  crystallite size can be completed by *ab initio* calculation of the diffracted intensity using the Debye equation in order to increase the precision of the measurement. Through the X-ray absorption spectroscopy, the local order around zinc atoms is identified having a spinel like structure and the low value for the number of zinc-zinc bonds situated at 3.50 Å reveals a weak occupation of tetrahedral site. Regarding the anomalous diffraction techniques, computer calculations of the scattered X-ray intensities have been performed on the zinc based phases. Using model aggregates of mixed  $\text{ZnSnO}$  entities, the salient features of the diffraction pattern have been identified and show that part of the zinc atoms are engaged in a  $\text{SnO}_2$  like structure.

Regarding the *in situ* experiments, the different results we have obtained on the two systems  $\text{ZnAl}_2\text{O}_4/\text{Al}_2\text{O}_3$  and  $\text{SnO}_2\text{-ZnAl}_2\text{O}_4/\text{Al}_2\text{O}_3$ , have shown the necessity to collect the data during the chemical process, the physico-chemical state of the catalyst being the same before and after the reaction. Taking into account the previous results obtained on the monoxide metal supported catalyst  $\text{ZnAl}_2\text{O}_4/\text{Al}_2\text{O}_3$ , we can assume thus that only a dramatic lack of occupancy on the metal site favours an incursion of light atoms in the network. Such behaviour can explain in return the expansion of the crystallographic cell as well as a significant increased of the Debye-Waller factor associated to zinc-zinc pairs.

### Acknowledgements

We express our thanks to J. M. Dubuisson and H. Sonnevile for *in situ* experiments and to E. Elkaim for help and discussion about anomalous X-ray diffraction.

### References

- [1] M.D. Amiridis, T. Zhang, R. J. Farrauto, *Appl. Catal. B* 10, 203 (1996).
- [2] V.I. Pârvulescu, P. Grange and B. Delmon, *Catal. Today* 46, 233 (1998).
- [3] M. Iwamoto, N. Mizumo, *J. Automot. Eng. (Part D)* 207, 23 (1993).
- [4] W. Held, A. Konig, T. Richter, L. Puppe, *Soc. Aut. Eng.* 900, 496 (1990).
- [5] W.F. Shangguan, Y. Teraoka, S. Kagawa, *Appl. Catal. B* 8, 217 (1996).
- [6] R. Revel, D. Bazin, E. Elkaim, H. Dexpert, Y. Kihn, *J. Phys. Chem. B* 104, 9828 (2000).
- [7] "X-ray Absorption : Principles, applications, techniques of Exafs, Sexafs and Xanes", Ed. Koningsberger, D. C. and Prins, R., (Ed.) J. Wiley, 1988.
- [8] D. Bazin, L. Guzzi, *Recent Res. Dev. Phys. Chem.* 3, 387 (1999).
- [9] D. Bazin, L. Guzzi, J. Lynch, *Applied Catalysis A* 226, 87 (2002).
- [10] J. L. Hodeau V. Favre-Nicolin, S. Bos, H. Renevier, E. Lorenzo, J.F. Berar, *Chem. Rev.* 101, 1843 (2001).
- [11] D. Bazin, D. Sayers, J. J. Rehr, *J. Phys. Chem B* 101, 11040 (1997).
- [12] B. S. Clausen *Catalysis Today*, 39, 293 (1998).
- [13] J. D. Grunwaldt, *Topics in Catalysis* 18(1), 37 (2002).
- [14] G. Sankar, J.M. Thomas, C.R.A. Catlow, *Topics in Catalysis* 10, 255 (2000).
- [15] T. Shido, R. Prins, *Current Opinion in Solid State and Mat. Sci.*, 3, 330 (1998).
- [16] "X ray Absorption Fine Structure for Catalysts and Surfaces", (Ed. : Y. Iwasawa), Ed. World Scientific 1996.
- [17] D. C. Koningsberger, B. L. Mojet, "Role and contributions of Xafs spectroscopy in catalysis", *Topics in catalysis*, 10 (2000).
- [18] A. Y. Stakheev, L. M. Kustov, *App. Catal. A* 188, 3 (1999).
- [19] K. J. Chao, A. C. Wei, *J. of Elec. Spec. and Rel. Phen.* 119, 175 (2001).
- [20] J. M. Thomas and W. J. Thomas, *Principles and practice of heterogeneous catalysis* (Ed. VCH, 1997).
- [21] J.W. Niemantsverdriet, *Topics in Catalysis* 8(1), 133 (1999).

- [22] R. Szymanski, P. Chaumette, CH. Travers, PH. Courty, D. Durand, *Stud. Surf. Sci. Cat.* 31, 739 (1987).
- [23] C. Chauvin, J. Saussey, J. C. Lavalley, H. Idriss, J. P. Hindermann, A. Kiennemann, P. Chaumette, P. Courty, *J. of Cat.* 121, 56 (1990).
- [24] G. Nicoli, R. Andouart, C. Barbier, D. Dagneaux, M. Desantis, D. Raoux, *Sociata Italiana Fisica, Conf. Proc.* 25, 353 (1990).
- [25] D. Bazin, L. Guzzi, *Recent Res. Dev. Phys. Chem.* 3, 387 (1999).
- [26] R. Revel, D. Bazin, A. Seigneurin, P. Barthe, J. M. Dubuisson, T. Descamps, H. Sonnevile, J. J. Poher, F. Maire, P. Lefrançois, *NIM B* 155, 183 (1999).
- [27] A. Michalowicz, Ph. D, Université Paris Val de Marne (1990).
- [28] M. Newville, B. Ravel, D. Haskel, J. J. Rehr, E. A. Stern, Y. Yacoby, *Physica B* 208-209, 154 (1995).
- [29] A. Michalowicz, G. Vlaic, *J. Synch. Rad.* 5, 1317 (1998).
- [30] A. Guinier, "Théorie et technique de la radiocristallographie », Ed. Dunod, Paris (1964).
- [31] B. E. Warren, *X-ray Diffraction*, Addison-Wesley : Reading, PA, (1969).
- [32] "Resonant anomalous X-ray scattering : theory and Applications " Ed. Materlik G., Sparks C., Fischer, K., Ed. North Holland (1994).
- [33] D. T. Cromer, J. B. Mann, *Acta. Crys. A* 24, 231 (1968).
- [34] S. Sasaki, KEK report 83-82, Nat. Lab. for High Energy Physics, Tsukuba, Japan (1983).
- [35] M.G. Samant, G. Bertgeret, G. Meitzner, P. Gallezot, M. Boudart, *J. Phys. Chem.* 92, 3542 (1988).
- [36] M.G. Samant, G. Bertgeret, G. Meitzner, P. Gallezot, M. Boudart, *J. Phys. Chem.* 86, 3547 (1987).
- [37] *Cerius Package, Insight User guide*, M.S.I., San Diego, 1995.
- [38] D. Bazin, R. Revel, *J. of Synchrotron Radiation* 6, 483, 1999.
- [39] D. E. Sayers, B. A. Bunker, in "*X-ray Absorption : Principles, Applications, Techniques of Exafs, Sexafs and Xanes*" ; Koningsberger, D. C. Prins, R. eds; John Wiley & Sons : New York, 1998, p 211.
- [40] J. J. Rehr and R. C. Albers, *Rev. Mod. Phys.* 72, 621, (2000).
- [41] J. J. Rehr, A. L. Ankudinov, *J. Syn. Rad.* 8, 61 (2001).
- [42] L. M. Coyler, G.N. Greaves, S.W. Carr, K.K. Fox, *J. Phys. Chem.* 101, 10105 (1997).
- [43] A. Winchell, H. Winchell, *Microscopic Caract. of Art. I norg. Sol. Sub.* 69 (1964).
- [44] D. Bazin, D. Sayers, *Jpn J. Appl. Phys.*, Vol. 32, Suppl. 32-2, 249 (1993).
- [45] D. Bazin, R. Revel, A. M. Flank, *J. of Syn. Rad.* 6, 717 (1999).
- [46] R. B. Greeger, F. W. Lytle, *J. of Cat.* 63, 476 (1980).
- [47] A. Jentys, *Phys. Chem. Chem. Phys.* 1(17), 4059 (1999).
- [48] Z. Wen Cheng, *Solid State Com.* 80, 213 (1991).
- [49] R. F. Cooley, J. S. Reed, *J of the Am. Ceram. Soc.* 5, 396 (1972).
- [50] A. M. Maltha, B. Brunet, J. Ziolkowski, J. Onishi, Y. Iwasawa, V. Ponec, *J. of Cat.* 356, 149 (1994).
- [51] J. Ziolkowski, A. M. Maltha, H. Kist, E. J. Grootendorst, H.J.M. Degroot, V. Ponec, *J. of Cat* 160, 148 (1996).
- [52] C. Oteroarean, B. Sintes Sintes, G. Turnes palominoturnes, C. Mas Carbonell, E. Escalona Platero, J. B. Parra Soto, *Microporous Materials* 8, 187 (1997).